Dispersion of Linear and Nonlinear Optical Susceptibilities in Calcium Neodymium Oxyborate $Ca_4NdO(BO_3)_3$—LDA versus GGA

Ali H. Reshak,*,† S. Auluck,‡ and I. V. Kityk§

Institute of Physical Biology, South Bohemia University, Institute of System Biology and Ecology, Academy of Sciences, Nove Hrady 37333, Czech Republic, Physics Department, Indian Institute of Technology Kanpur, Kanpur (UP) 208016, India, and Electrical Engineering Department, Technological University of Czestochowa, Al.Armii Krajowej 17/19, Czestochowa, Poland

Received: November 8, 2008; Revised Manuscript Received: December 16, 2008

We have performed ab inito theoretical calculations of the electronic structure and the linear and nonlinear optical susceptibilities for calcium neodymium oxyborate $Ca_4NdO(BO_3)_3$ using two approximations for the exchange correlation (XC) potentials, the local density approximation (LDA) and the generalized gradient approximation (GGA). Our calculations show that this compound is metallic-like, with density of states at the Fermi energy E_F, $N(E_F)$, of 5.95 and 10.33 states/Ry-cell or bare electronic specific heat coefficients of 1.03 and 1.79 mJ/mol-K^2 for LDA and GGA, respectively. The overlap between the valence and conduction bands is strong, resulting in metallic behavior. We found that Nd-s/p/d, Ca-s/p, B-p, and O-s/p states controlled the overlapping around E_F. The effect of LDA and GGA on the band structure, density of states, and linear optical properties is very small, while for the nonlinear optical properties, it is very pronounced. Our calculations show that $\chi^{(2)}_{111}(\omega)$ is the dominant component for both LDA and GGA. We find opposite signs of the contributions of the 2ω and 1ω inter/intraband to the real and imaginary parts for the dominant component throughout the wide optical frequency range.

1. Introduction

The increasing variety of applications of nonlinear optical materials for second harmonic generation (SHG), sum or difference frequency mixing, optical parametric oscillation, or amplification has resulted in the development of inorganic nonlinear optical crystals.[1] The development of highly efficient nonlinear optical crystals for the ultraviolet region is extremely important for both laser spectroscopy and laser processing, including laser tailoring of molecules and optical triggering. In particular, the borate crystals are very useful for solid-state ultraviolet lasers[2–4] and the infrared spectral range. The number of well-characterized solid alkaline earth-rare-earth borates is so far very small and includes the Sr^{2+}-containing phase $Sr_3R_2(BO_3)_4$ (see, e.g., Abdullaev and Mamedov[5]) and the Ba^{2+}-containing phase[6] with similar compostion, $Ba_3R_2(BO_3)_4$, but with different structure.[7] Another family of oxyborates, with the composition $A_6MM'(BO_3)_6$, where A = Sr or Ba, has been found.[8,9] The metal ions M and M′ comprise several metal ions, whose sum of formal charges adds up to +6. In general, rare-earth borates containing, among others, Nd could be of greater importance as they might be a potential miniature laser material.[6] The nonlinear optical properties of the oxoborate family have been reported and appear to be comparable to those of β-BaB_2O_4 (BBO) for SHG.[1] By studying the structural charactrization of the borate crystals, we can understand why the borate crystals dominate in the field of the nonlinear optics. The boron atom has two types of hybridized orbitals, the planar sp^2 and the three-dimensional sp^3, to coordinate three or four oxygen atoms forming BO_3^{4-} or BO_4^{5-} clusters. Further, these clusters can comprise several different typical B_xO_y groups, and therefore, various types of borate crystals can be constructed based on these infrastructures, for example, the isolated BO_3 group in NAB and CReOB, the B_3O_6 group in BBO, the B_3O_7 group in LBO, and the B_5O_{10} group in KB_5. This is a very attractive phenomenon discovered in inorganic borate crystals. Therefore, it is very interesting to study the influence of these BO_3^{4-} or BO_4^{5-} clusters on the second-order NLO response of various types of borate crystals, so that we can get some useful information in searching for new NLO materials.[1]

The optical properties of solids are a major topic, both in basic research as well as for industrial applications. While for the former the origin and nature of different excitation processes is of fundamental interest, the latter can make use of them in many optoelectronic devices. These wide interests require experiment and theory. To the best of our knowledge, there are no experimental measurements and also no first-principles calculations of the linear and nonlinear optical properties of calcium neodymium oxyborate $Ca_4NdO(BO_3)_3$. Therefore, we thought it was worthwhile to perform a theoretical study of this compound. We address ourselves to a detailed comparison of two approximations for the exchange correlation (XC) potentials, the local density approximation (LDA) and the generalized gradient approximation (GGA).

The second section describes the methods used for the theoretical calculations of linear and nonlinear optical susceptibilities. The third section presents principal results concerning the dispersion of linear and nonlinear optical susceptibilities and discussion of the obtained results.

* To whom correspondence should be addressed. Tel.: +420 777729583. Fax: +420-386 361231. E-mail address:maalidph@yahoo.co.uk.
† South Bohemia University and Academy of Sciences.
‡ Indian Institute of Technology Kanpur.
§ Technological University of Czestochowa.

10.1021/jp8098522 CCC: $40.75
Published on Web 02/05/2009

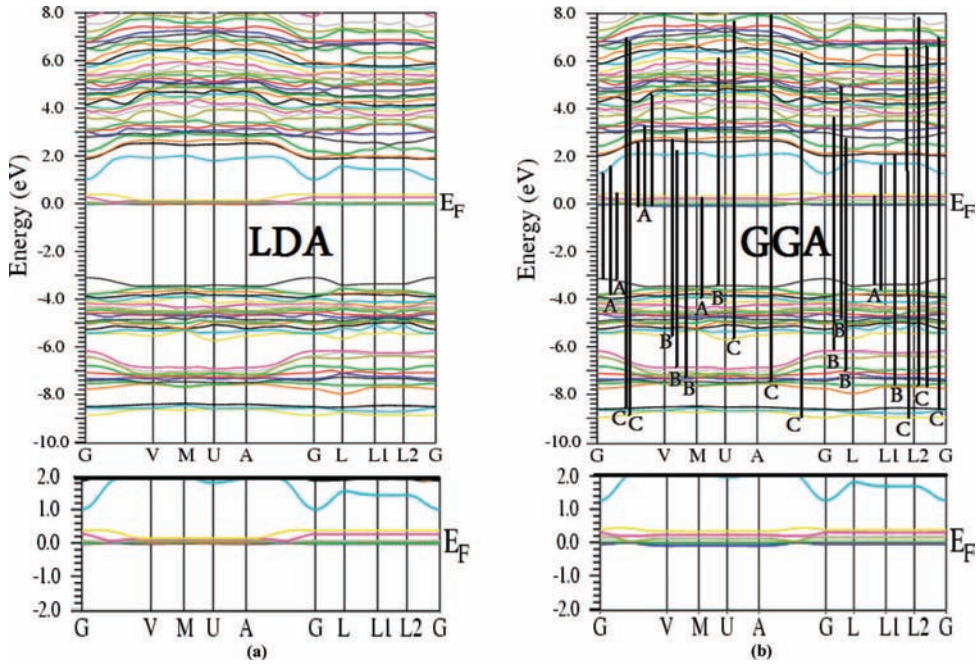

Figure 1. (a) The band structure using LDA along with the enlarged part around E_F. (b) The band structure using GGA, along with the enlarged part around E_F.

2. Theoretical Calculation

We have performed calculations of the electronic band energy structure and the optical susceptibilities applying the full potential linearized augmented plane wave (FP-LAPW) method as incorporated in WIEN2K code.[10] This is an implementation of the density functional theory (DFT)[11] with different possible approximations for the exchange correlation (XC) potentials. The exchange correlation potential was calculated using the local density approximation (LDA) and the generalized gradient approximation (GGA) PBE.[12] In order to achieve desirable energy eigenvalue convergence, the wave functions in the interstitial regions were expanded in plane waves with a cutoff of $K_{max} = 9/R_{MT}$, where R_{MT} denotes the smallest atomic sphere radius and K_{max} gives the magnitude of the largest K vector in the plane wave expansion. The muffin tin radii were assumed to be 2.25 and 2.06 atomic units (au) for Nd and Ca, respectively, and 1.31 au for B and O. The valence wave functions inside of the spheres were expanded up to $l_{max} = 10$, while the charge density was Fourier expanded up to $G_{max} = 14$ $(au)^{-1}$. Self-consistency was achieved using 350 k points in the irreducible Brillouin zone (IBZ). The IBZ integration was carried out numerically using the tetrahedron method.[13,14] The linear optical properties were calculated using 500 k points, and the nonlinear optical properties were calculated using 1500 k points in IBZ. The calculations were assumed to be converged when the total energy of the system was stabilized within 10^{-5} Ry.

3. Results and Discussion

3.1. Band Structure and Density of States. We present the band structure and the total and partial density of states (DOS) using LDA and GGA in Figures 1 and 2. These figures suggest that the band structure and the DOS can be divided into five distinct spectral groups/structures. We have enlarged the band structure near E_F in order to show the overlapping of the bands around E_F. We found that Nd-s/p/d/f, Ca-s/p, B-p, and O-s/p states controlled the overlapping around E_F. The DOS at the Fermi energy (E_F) is determined by the overlap between the valence and conduction bands. This overlap is strong enough, indicating a metallic-like origin with DOS at E_F, $N(E_F)$, of 5.95 and 10.33 states/Ry-cell, for LDA and GGA, respectively. Although the band structure and DOS obtained within LDA and GGA are very similar, the DOS at E_F, $N(E_F)$, are very different. The electronic specific heat coefficient (γ), which is function of density of states, can be calculated using the expression

$$\gamma = \frac{1}{3}\pi^2 N(E_F) k_B^2 \quad (1)$$

Here, $N(E_F)$ is the density of states at the Fermi energy, and k_B is the Boltzmann constant. The calculated density of states at the Fermi energy $N(E_F)$ enables us to calculate the bare electronic specific heat coefficient, which is found to be 1.03 and 1.79 mJ/mol-K^2 for LDA and GGA, respectively. We hope that future experiments will help in determining which of the approximations (LDA or GGA) is better.

From the PDOS, we are able to identify the angular momentum character of the various structures. The lowest group (first group), which is located at −9.0 eV, is mainly from O1-s, O2-s/p, O3-s/p, O4-s/p, O5-s/p, O6-s/p, and B-s states, with a small contribution from Ca-s/p and Nd-s/p/d states. The second group (−8.0 to −6.0 eV) is mainly from O1-s, O2-s/p, O3-s/p, O4-s/p, O5-s/p, O6-s/p, Nd-s/p/d, B1-s/p, B2-s/p, Ca1-s/p, and Ca2-s/p states. The third group (−6.0 to −3.0 eV) is a mixture of O1-p, O2-p, O3-p, O4-p, O5-s/p, O6-s/p, Ca1-s/p, Ca2-s/p, B1-p, B2-p, and Nd-s/p/d states. The group around the Fermi energy consists of O1-s/p, O2-s/p, O4/p, O5-p, O6-s/p Ca-s/p, Ca2-s/p, B1-p, and Nd-s/p/d/f states. The last group from the Fermi energy and above is a mixture of Ca1-s/p, Ca2-s/p, B1-s/p, B2-s/p, Nd-s/p/d, and -s/p states of all O atoms.

From the PDOS, we note that there is a strong hybridization between the states. Nd-s and Nd-p hybridize strongly in the energy range from the Fermi energy and above, Nd-d with Nd-p in the energies from −9.0 to −4.0 eV, Nd-s with Ca1-s in the energies from −9.0 to −4.0 eV and from 2.0 eV and above, Ca1-p with Ca1-s and Nd-s in the energies from 2.0 eV and

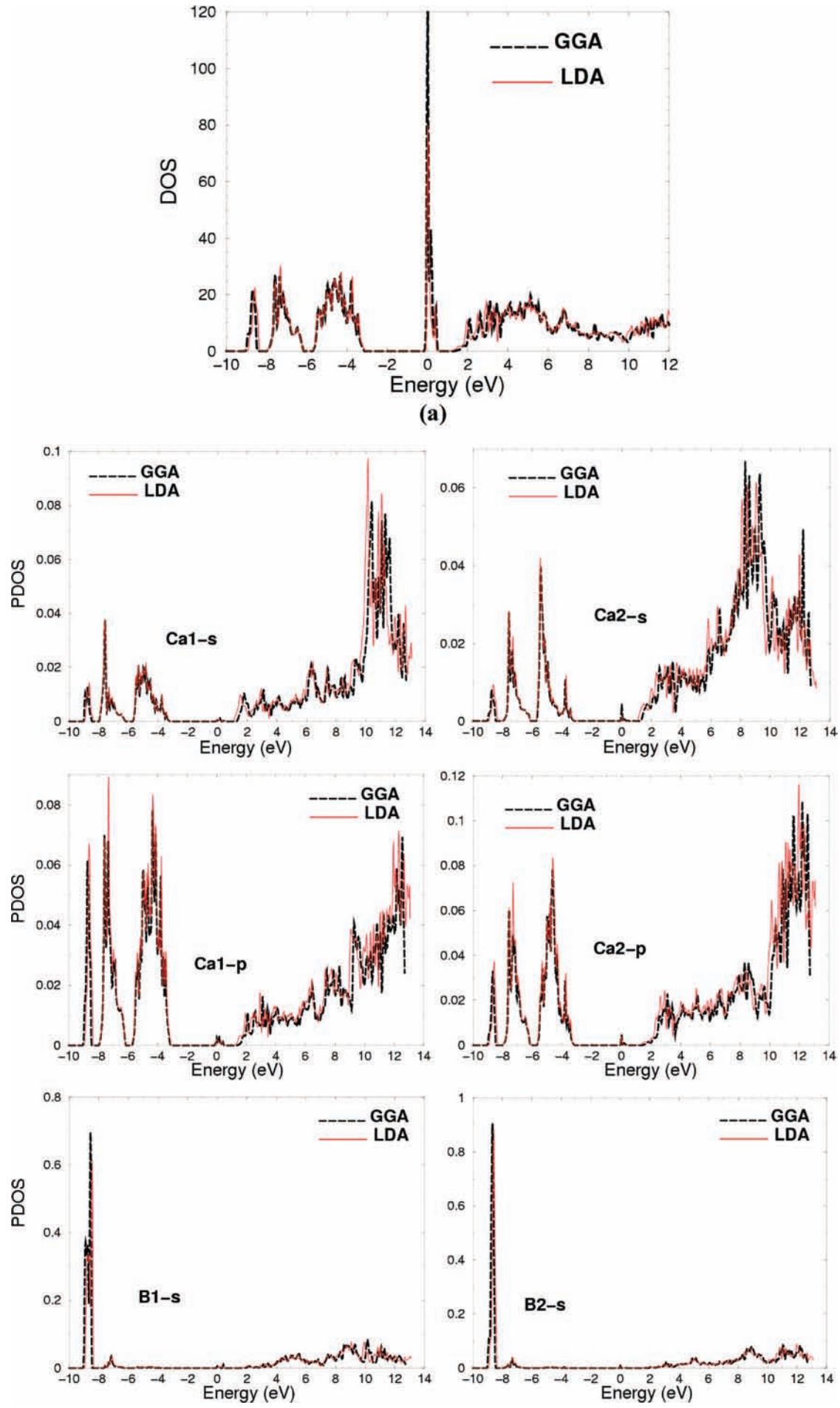

Figure 2A. Part 1 of 4.

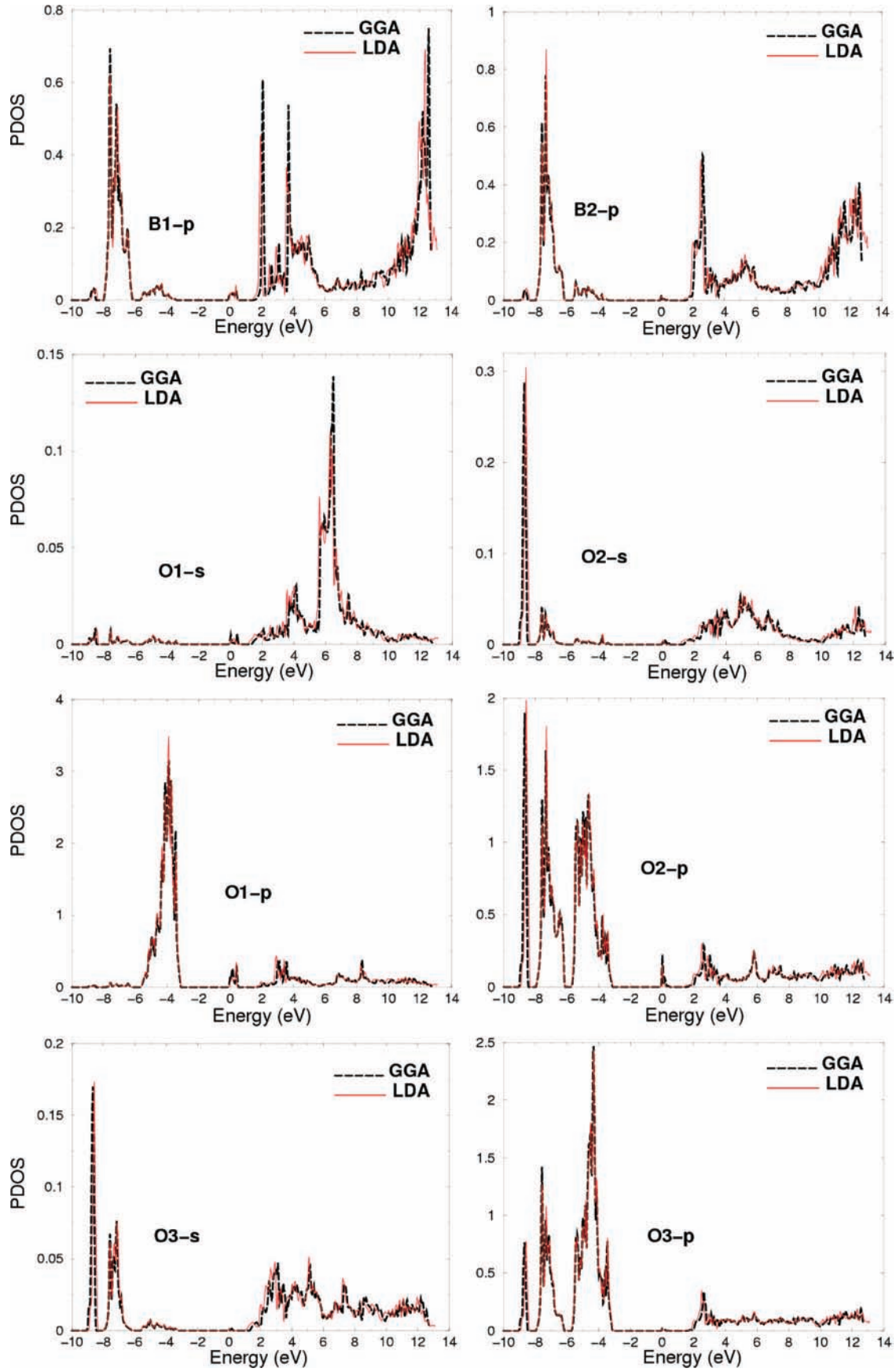

Figure 2B. Part 2 of 4.

above, Ca1,2-s with Nd-d in the energies from −9.0 to −4.0 eV, Ca2-s with Ca1-s and Nd-s in the energies from −9.0 to −4.0 eV, Ca2-s with Nd-d in the energies from 2.0 to 6.0 eV, Ca2-p with Nd-d in the energies from −9.0 to −4.0 eV, O1-p with Nd-p at around −9.0 eV, B1-s with Nd-p, all O-p and O2-s at around 9.0 eV, B1-p with O2-p and O3-s/p in the

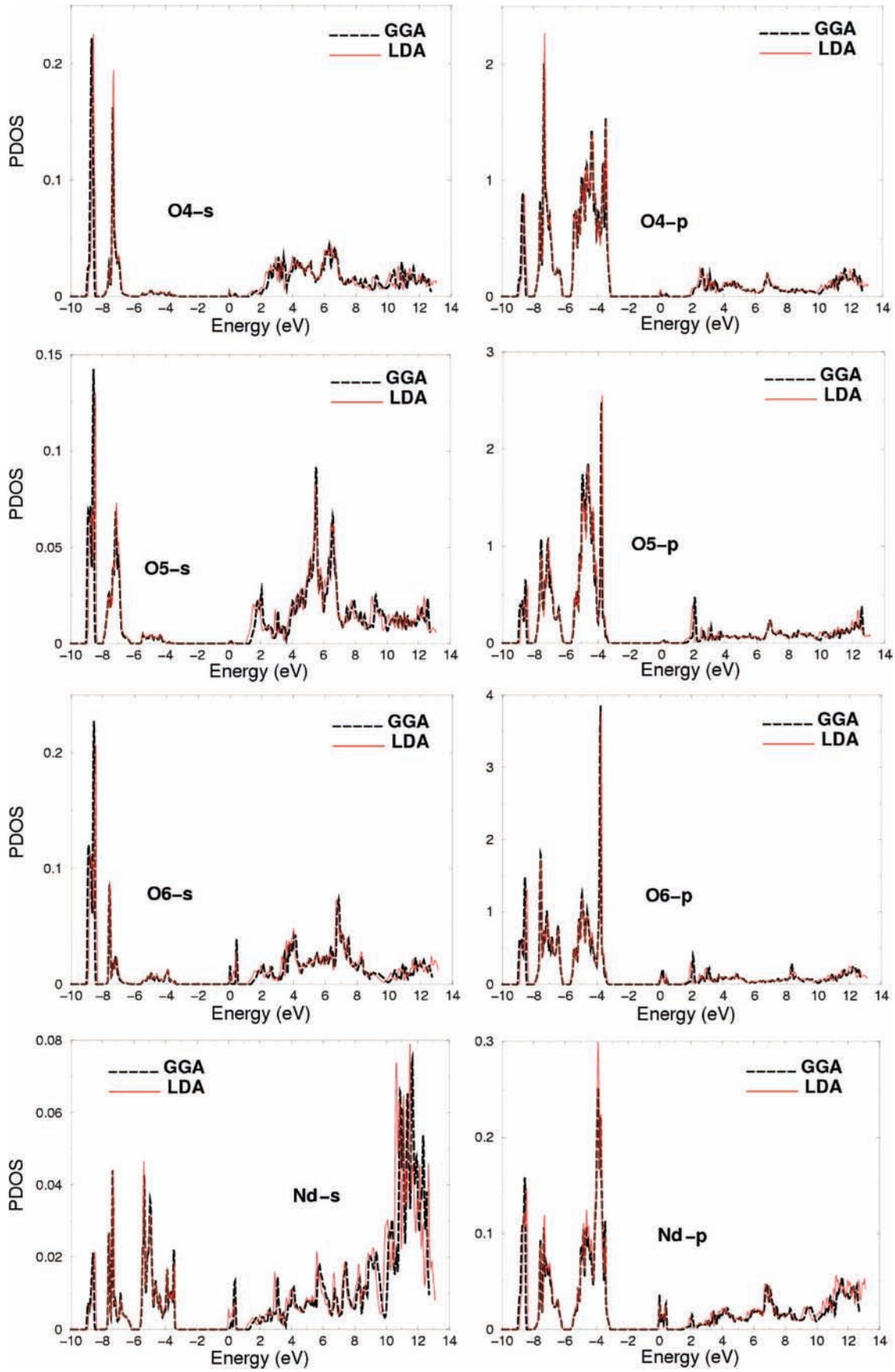

Figure 2C. Part 3 of 4.

energies from −8.0 to −6.0 eV, B1-p with all O-s/p at around 2.0 eV, B1-p with Ca1,2-p at around −9.0 eV and in the energies from −6.0 to −4.0 eV.

3.2. First-Order (Linear) Optical Susceptibilities. The interband transitions of the dielectric function $\varepsilon(\omega)$ can be split into direct and indirect transitions. We neglect the indirect

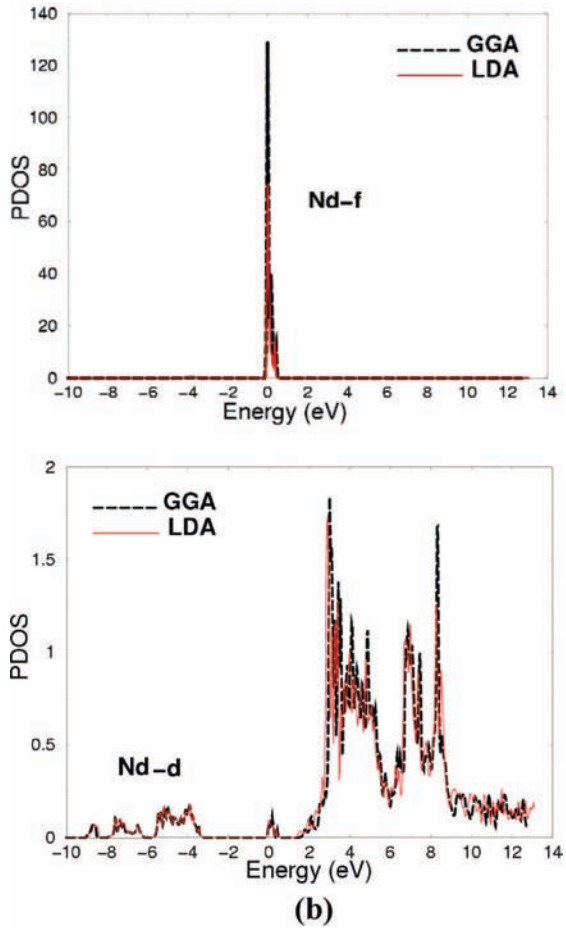

Figure 2D. Part 4 of 4. (a) Top panel of (A): Calculated total densities of states (states/eV unit cell) for calcium rare-earth oxyborates $Ca_4NdO(BO_3)_3$ using LDA and GGA. (b) (A—D): Calculated partial densities of states (states/eV unit cell).

interband transitions involving scattering of phonons that are expected to give a small contribution to $\varepsilon(\omega)$ for the case of the borates.[15] To calculate the direct interband contributions to the imaginary part of the dielectric function $\varepsilon_2(\omega)$, it is necessary to sum up all possible transitions from the occupied to the unoccupied states. Taking the appropriate transition matrix elements into account, we calculated the imaginary part of the dielectric functions $\varepsilon_2(\omega)$ using the expressiosns[16,17]

$$\varepsilon_2^{\parallel}(\omega) = \frac{12}{m\omega^2}\int_{BZ}\sum\frac{|P^Z_{nn'}(k)|^2 dS_k}{\nabla\omega_{nn'}(k)} \quad (2a)$$

$$\varepsilon_2^{\perp}(\omega) = \frac{6}{m\omega^2}\int_{BZ}\sum\frac{[|P^X_{nn'}(k)|^2 + |P^Y_{nn'}(k)|^2] dS_k}{\nabla\omega_{nn'}(k)} \quad (2b)$$

The above expressions are written in atomic units with $e^2 = 1/m = 2$ and $\hbar = 1$, where ω is the photon energy and $P^X_{nn}(k)$ is the X component of the transition dipole matrix elements between initial $|nk\rangle$ and final $|n'k\rangle$ band states with their eigenvalues $E_n(k)$ and $E_{n'}(k)$, respectively. The $\omega_{nn'}(k)$ is the energy difference $\omega_{nn'}(k) = E_n(k) - E_{n'}(k)$, and S_k is a constant energy surface $S_k = \{k;\omega_{nn'}(k) = \omega\}$. The integration is done over the first IBZ. For the metallic materials, there are two contributions to $\varepsilon(\omega)$, namely, intraband and interband transitions. As the investigated compound is metallic, we must include the Drude term (intraband transitions)[18]

$$\varepsilon_2^{\perp}(\omega) = \varepsilon^{\perp}_{2inter}(\omega) + \varepsilon^{\perp}_{2intra}(\omega) \quad (3)$$

where

$$\varepsilon^{\perp}_{2intra}(\omega) = \frac{\omega_P^{\perp}\tau}{\omega(1+\omega^2\tau^2)}$$

where $\omega_P$is the anisotropic plasma frequency[19] and τ is the mean free time between collisions

$$\omega_P^{\perp 2} = \frac{8\pi}{3}\sum_{kn}\vartheta^{\perp 2}_{kn}\delta(\varepsilon_{kn}) \quad (4)$$

where ε_{kn} is $E_n(k) - E_F$ and $\vartheta^{\perp}_{kn}$ is the electron velocity (in the basal plane). Similar expressions for the parallel component can be written.

Figure 3a—c displays the variation of the imaginary (absorptive) part of the electronic dielectric function $\varepsilon_2(\omega)$ for both LDA and GGA. The broadening is taken to be 0.1 eV so as bring out all of the structures.[26] The calculated imaginary part $\varepsilon_2(\omega)$ can be used to describe the transitions between the occupied and unoccupied bands. It can be seen from $\varepsilon_2(\omega)$ spectra that the strong peaks are located at energies of 7.0, 9.0, 11.0 eV and 7.0—8.0 eV for $\varepsilon_2^{XX}(\omega)$ and $\varepsilon_2^{ZZ}(\omega)$, respectively, for GGA calculation. The corresponding peaks in the LDA calculation occur at energies 0.1—0.2 eV lower. The magnitude of the peaks is different for LDA and GGA. We should emphasize that there is a considerable anisotropy between $\varepsilon_2^{XX}(\omega)$ and $\varepsilon_2^{ZZ}(\omega)$ (Figure 3c). At energies less than 2.0 eV and between 10.0 and 12.0 eV, $\varepsilon_2^{XX}(\omega)$ shows a larger contribution, and between 4.5 and 9.0 eV, $\varepsilon_2^{ZZ}(\omega)$ is the dominant, whereas at higher energies both polarizations contribute.

We have performed calculations of $\varepsilon_2^{XX}(\omega)$ and $\varepsilon_2^{ZZ}(\omega)$ with and without the inclusion of the Drude term. The effect of the Drude term is significant for energies less than 1 eV. The sharp rise at low energies is due to the Drude term. The peaks in the optical response are caused by the allowed electric dipole transitions between the valence and conduction bands. In order to identify these structures, we should consider the magnitude of the optical matrix elements. The observed structures would correspond to those transitions which have large optical matrix dipole transition elements. It would be worthwhile to attempt to identify the band transitions that are responsible for the spectral structures in $\varepsilon_2^{XX}(\omega)$ and $\varepsilon_2^{ZZ}(\omega)$ using our calculated band structure. Figure 1b presents the optical transitions which are responsible for the spectral structures in $\varepsilon_2^{XX}(\omega)$ and $\varepsilon_2^{ZZ}(\omega)$. For simplicity, we have labeled the transitions in Figure 1b as A, B, and C. The transitions A are responsible for the structures in $\varepsilon_2^{XX}(\omega)$ and $\varepsilon_2^{ZZ}(\omega)$ for energies up to 5.0 eV, transitions B are responsible for the structures in the energy range of 5.0—10.0 eV, and the transitions C are responsible for the structures between 10.0 and 14.0 eV.

From the imaginary parts of the dielectric function $\varepsilon_2^{XX}(\omega)$ and $\varepsilon_2^{ZZ}(\omega)$, the real parts $\varepsilon_1^{XX}(\omega)$ and $\varepsilon_1^{ZZ}(\omega)$ can be calculated using Kramers—Kronig relations.[20] The calculated optical conductivity $\sigma(\omega)$ components are shown in Figure 3d. There is no significant difference between the two approximations (LDA and GGA).

3.3. Second-Order Optical Susceptibilities. The complex second-order nonlinear optical susceptibility tensor can be generally written as $\chi^{(2)}_{ijk}(-2\omega;\omega;\omega)$; for simplicity, we denote $\chi^{(2)}_{ijk}(-2\omega;\omega;\omega)$ as $\chi^{(2)}_{ijk}(\omega)$.[23—25] The subscripts i, j, and k are the Cartesian indices. The structural analysis showed that calcium neodymium oxyborate $Ca_4NdO(BO_3)_3$ crystallizes in the monoclinic space group 8_*Cm*. On the basis of this symmetry group, there are 10 third-order independent tensor components of the second-order susceptibility tensor determining SHG, namely, $\chi^{(2)}_{111}(\omega)$, $\chi^{(2)}_{121}(\omega)$, $\chi^{(2)}_{122}(\omega)$, $\chi^{(2)}_{133}(\omega)$, $\chi^{(2)}_{211}(\omega)$, $\chi^{(2)}_{212}(\omega)$, $\chi^{(2)}_{222}(\omega)$, $\chi^{(2)}_{233}(\omega)$, $\chi^{(2)}_{313}(\omega)$, and $\chi^{(2)}_{323}(\omega)$ (1, 2, and 3 refer to the x, y, and z axes,

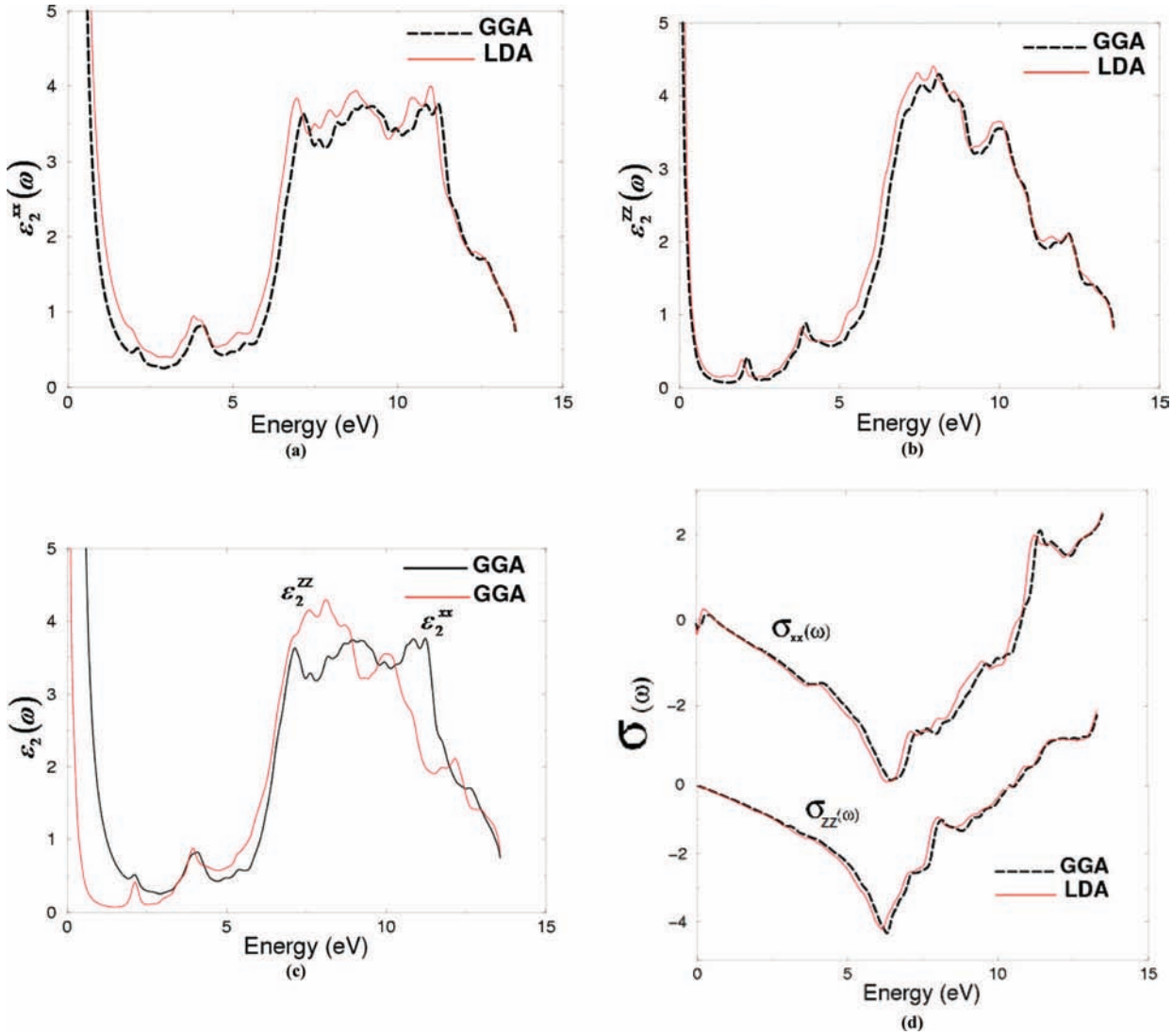

Figure 3. (a) Calculated $\varepsilon_2^{XX}(\omega)$ using LDA and GGA. (b) Calculated $\varepsilon_2^{ZZ}(\omega)$ using LDA and GGA. (c) Calculated $\varepsilon_2^{XX}(\omega)$ and $\varepsilon_2^{ZZ}(\omega)$ using GGA. (d) Calculated $\sigma(\omega)$ spectrum.

TABLE 1: Calculated Total Real Part of the $\chi_{ijk}^{(2)}(0)$ at Zero Frequency for LDA* and GGA Calculations**

	$\chi_{111}^{(2)}(0)$	$\chi_{121}^{(2)}(0)$	$\chi_{122}^{(2)}(0)$	$\chi_{133}^{(2)}(0)$	$\chi_{211}^{(2)}(0)$	$\chi_{212}^{(2)}(0)$	$\chi_{222}^{(2)}(0)$	$\chi_{233}^{(2)}(0)$	$\chi_{313}^{(2)}(0)$	$\chi_{323}^{(2)}(0)$
10^{-7} esu	-1.1^{*}	-1.09^{*}	0.5^{*}	0.11^{*}	0.3^{*}	-0.08^{*}	0.1^{*}	0.09^{*}	-0.05^{*}	-0.009^{*}
	-1.4^{**}	-1^{**}	0.39^{**}	0.1^{**}	0.28^{**}	-0.05^{**}	0.09^{**}	0.075^{**}	-0.03^{**}	-0.005^{**}
10^{-12} pm/V	-45^{*}	-45^{*}	21^{*}	4.3^{*}	12^{*}	-2.8^{*}	3.9^{*}	3.4^{*}	-1.4^{*}	-0.5^{*}
	-60^{**}	-42^{**}	16^{**}	4.5^{**}	11^{**}	-2.4^{**}	3.7^{**}	3.1^{**}	-1.2^{**}	-0.3^{**}

respectively).[21] We have calculated the total complex susceptibility of all 10 components of SHG using LDA and GGA. We have established that $\chi_{111}^{(2)}(\omega)$ is the dominant component, giving the highest value of the total $\mathrm{Re}[\chi_{111}^{(2)}(0)]$ of about -1.1×10^{-4} and -1.4×10^{-7} esu, for both LDA and GGA (Table 1) in comparison with the other components. The calculated imaginary part of the second-order SHG susceptibilities in the energy range between 0.0 and 3.0 eV is shown in Figure 4a for both LDA and GGA. The difference between the two approximations is very pronounced. This is attributed to the fact that the nonlinear optical susceptibilities are more sensitive to small changes in the band structure than the linear optical one. Hence, any anisotropy in the linear optical properties is enhanced more significantly in the nonlinear spectra, as illustrated in Figure 4a. We hope that future experiments will help in deciding which approximation is better. The real part of the SHG tensors for the dominant component for both LDA and GGA calculations is shown in Figure 4b.

Figure 5a,b shows the 2ω and 1ω inter/intraband contributions to the real and imaginary parts of the dominant component of the SHG tensor $\chi_{111}^{(2)}(\omega)$. We should emphasize the opposite signs of the two contributions throughout the frequency range. This fact may be used in the future for molecular engineering of the crystals in the desirable directions. The lack of experimental data prevents any conclusive comparison with experiment over a large spectral energy range. A definite enhancement in the anisotropy upon going from linear optical properties to the nonlinear optical properties is evident (Figure 4c).

One could expect that the spectral structures in $\mathrm{Im}[\chi_{ijk}^{(2)}(\omega)]$ could be understood from the features of $\varepsilon_2(\omega)$. Unlike the linear optical spectra, the features in the SHG susceptibility are very difficult to identify from the band structure because of the presence of 2ω and ω resonance terms. We could still use the linear optical spectra to identify the different resonances leading to various features in the SHG spectra. The first spectral band in $\mathrm{Im}[\chi_{111}^{(2)}(\omega)]$ between 0.0 and 1.0 eV originates from the 2ω

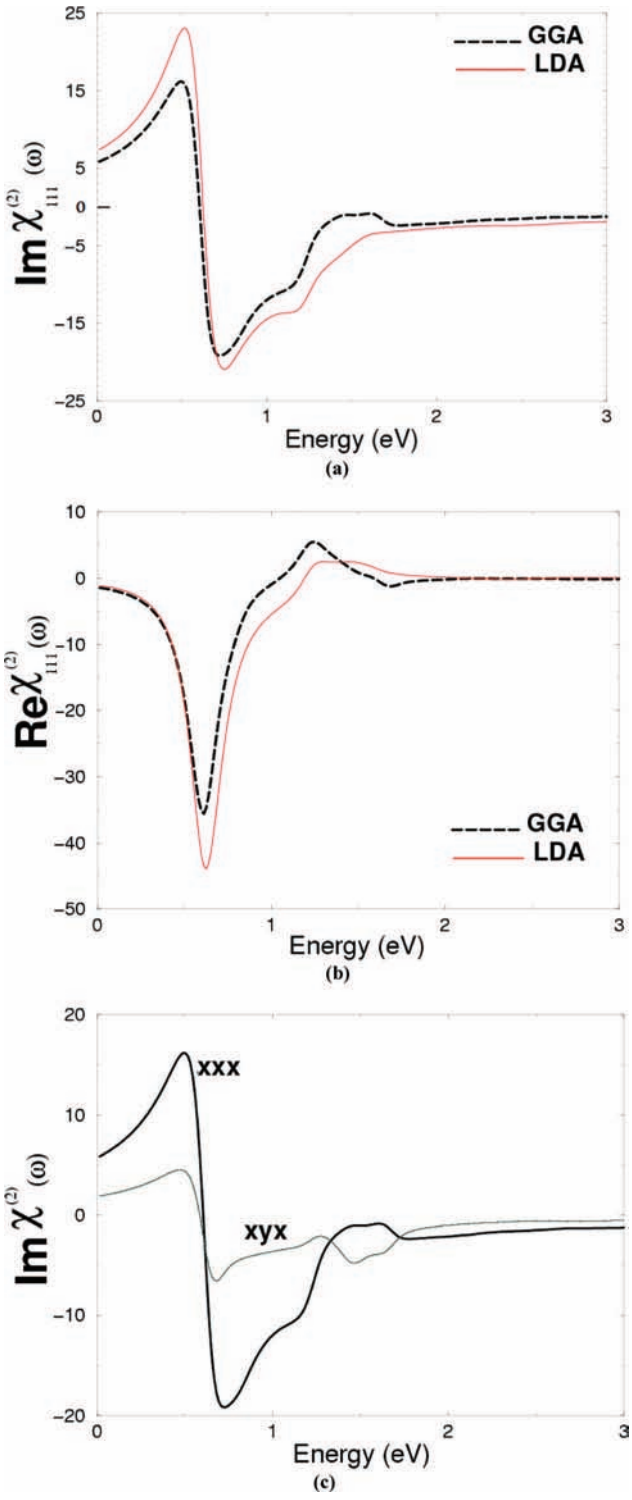

Figure 4. The calculated complex second-order nonlinear optical susceptibility tensor for the dominant component $\chi^{(2)}_{111}(\omega)$ using LDA and GGA, (a) imaginary part of $\chi^{(2)}_{111}(\omega)$, (b) real part of $\chi^{(2)}_{111}(\omega)$, (c) definite enhancement in the anisotropy between $\chi^{(2)}_{111}(\omega)$ and $\chi^{(2)}_{121}(\omega)$. All $\chi^{(2)}(\omega)$ are multiplied by 10^{-7}, in esu units.

resonance and arises from the first structural maximum in $\varepsilon_2(\omega)$. The second spectral band between 1.0 and 2.0 eV is associated with interference between the ω resonance and the 2ω resonance and is associated with the high-energy structure in $\varepsilon_2(\omega)$. The last structure from 2.0 to 3.0 eV is mainly due to ω resonance and is associated with the tail in $\varepsilon_2(\omega)$. The obtained data show that existence of Nd^{3+} ions in the crystalline matrix may give

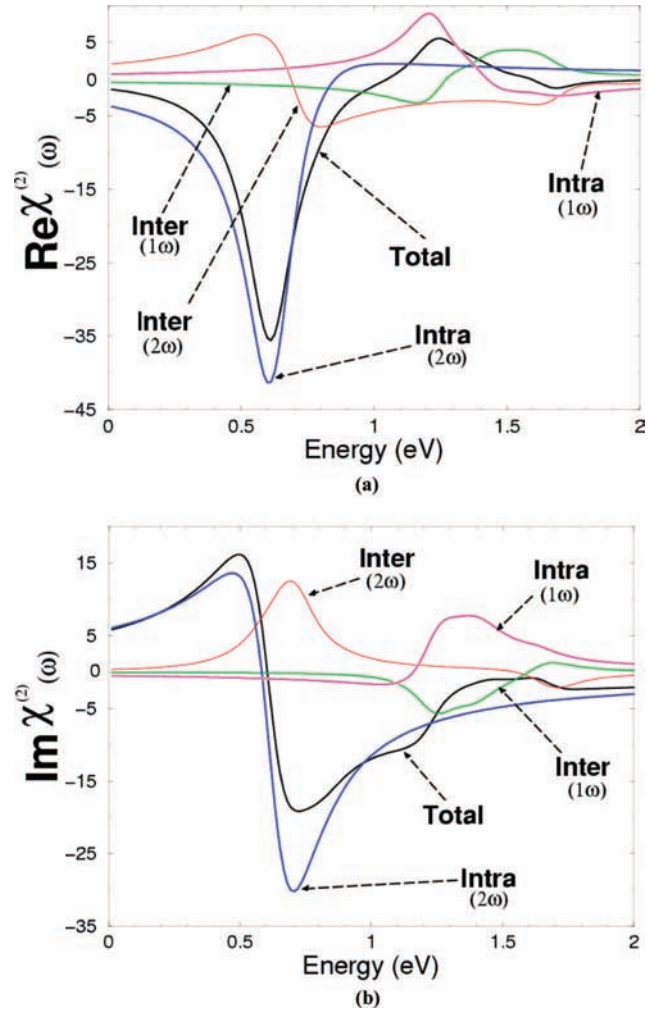

Figure 5. Calculated total Re[$\chi^{(2)}_{111}(\omega)$] and Im[$\chi^{(2)}_{111}(\omega)$] spectrum along with the intra $(2\omega)/(1\omega)$ and inter $(2\omega)/(1\omega)$-band contributions. Re and Im[$\chi^{(2)}(\omega)$] are multiplied by 10^{-7}, in esu units.

several differences with respect to the borate crystals without other rare-earth ions.[22]

4. Conclusions

The electronic band energy structure and the linear and nonlinear optical susceptibilities have been studied theoretically for calcium neodymium oxyborate $Ca_4NdO(BO_3)_3$ using LDA and GGA. Our calculations show the following. (1) This compound is metallic-like. (2) The DOS at the Fermi energy (E_F) is determined by the overlap between the valence and conduction bands. This overlap is strong enough, indicating a metallic-like origin with DOS at E_F, $N(E_F)$, of 5.95 and 10.33 states/Ry-cell for LDA and GGA, respectively. (3) We have performed calculations of $\varepsilon_2^{XX}(\omega)$ and $\varepsilon_2^{ZZ}(\omega)$ with and without the inclusion of the Drude term. The effect of the Drude term is significant for energies less than 1 eV. The sharp rise at low energies is due to the Drude term. (4) The complex second-order nonlinear optical susceptibility tensor has been calculated for the SHG tensors $\chi^{(2)}_{111}(\omega)$, $\chi^{(2)}_{121}(\omega)$, $\chi^{(2)}_{122}(\omega)$, $\chi^{(2)}_{133}(\omega)$, $\chi^{(2)}_{211}(\omega)$, $\chi^{(2)}_{212}(\omega)$, $\chi^{(2)}_{222}(\omega)$, $\chi^{(2)}_{233}(\omega)$, $\chi^{(2)}_{313}(\omega)$, and $\chi^{(2)}_{323}(\omega)$ using LDA and GGA. (5) We find that $\chi^{(2)}_{111}(\omega)$ is the dominant component giving the highest value of the total Re[$\chi^{(2)}_{111}(0)$] (about -1.1×10^{-4} and -1.4×10^{-7} esu for LDA and GGA, respectively). (6) We have presented the 2ω and 1ω inter/intraband contributions to the real and imaginary parts of the dominant SHG component.

We would like to emphasize the opposite signs of the two contributions throughout the wide energy range. This fact may be used in the future for molecular engineering of the crystals in the desirable directions.

Acknowledgment. This work was supported from the institutional research concept of the Institute of Physical Biology, UFB (No.MSM6007665808), and the Institute of System Biology and Ecology, ASCR (No. AVOZ60870520).

References and Notes

(1) Xue, D.; Zhang, Z. *Appl. Phys. A: Mater. Sci. Process.* **1999**, *68*, 57–61.

(2) Ramachandra, R. C.; Gobinathan, R.; Gnanan, F. D. *Cryst. Res. Technol.* **1993**, *28*, 737.

(3) Chen, C.; Wang, Y.; Xia, Y.; Wu, B.; Tang, D.; Wu, K.; Zeng, W.; Yu, L.; Mei, L. *J. Appl. Phys.* **1995**, *77*, 2268.

(4) Mori, Y.; Kuroda, I.; Nakajima, S.; Sasaki, T.; Nakai, S. *Appl. Phys. Lett.* **1995**, *67*, 1818.

(5) Abdullaev, G. K.; Mamedov, K. S. *Kristallografiya* **1982**, *27*, 795.

(6) Yan, J. F.; Hone, H. Y.-P. *Mater. Res. Bull.* **1987**, *22*, 1347.

(7) Norrestam, R.; Nygren, M.; Bovin, J.-O. *Chem. Mater.* **1992**, *4*, 737–743.

(8) Thompson, P.; Keszler, D. A. *Chem. Mater.* **1989**, *1*, 292.

(9) Schaffers, K. I.; Alekel, T.; Thompson, P. D.; Cox, J. R.; Keszler, D. A. *Chem. Mater.* **1989**, *1*, 7068.

(10) Blaha, P.; Schwarz, K.; Madsen, G. K. H.; Kvasnicka, D.; Luitz, J. *WIEN2K, An Augmented Plane Wave + Local Orbitals Program for Calculating Crystal Properties*; Karlheinz Schwarz Techn. Universitat: Wien, Austria, 2001; ISBN 3-9501031-1-2.

(11) Hohenberg, P.; Kohn, W. *Phys. Rev. B* **1964**, *136*, 864.

(12) Perdew, J. P.; Burke, S.; Ernzerhof, M. *Phys. Rev. Lett.* **1996**, *77*, 3865.

(13) (a) Jepsen, O.; Andersen, O. K. *Solid State Commun.* **1971**, *9*, 1763. (b) Lehmann, G.; Taut, M. *Phys. Status Solidi B* **1972**, *54*, 496.

(14) Wilson, J. A.; Yoffe, A. D. *Adv. Phys.* **1969**, *18*, 193.

(15) Smith, N. V. *Phys. Rev. B* **1971**, *3*, 1862.

(16) (a) Hufner, S.; Claessen, R.; Reinert, F.; Straub, Th.; Strocov, V. N.; Steiner, P. *J. Electron Spectrosc. Relat. Phenom.* **1999**, *100*, 191. (b) Ahuja, R.; Auluck, S.; Johansson, B.; Khan, M. A. *Phys. Rev. B* **1994**, *50*, 2128.

(17) Reshak, A. H.; Kityk, I. V.; Auluck, S. *J. Chem. Phys.* **2008**, *129*, 074706.

(18) Wooten, F. *Optical Properties of Solids*; Academic Press: New York, 1972.

(19) Chakraborrty, B.; Pickett, W. E.; Allen, P. B. *Phys. Rev. B* **1972**, *14*, 3227.

(20) Tributsch, H.; Naturforsch, Z. *Z. Naturforsch., A: Phys. Sci.* **1977**, *32*, 972.

(21) Boyd W. *Nonlinear Optics*; Academic Press: Boston, MA, 1992.

(22) Reshak, A. H.; Auluck, S.; Majchrowski, A.; Kityk, I. V. *Solid State Sci.* **2008**, *10*, 1445–1448.

(23) Reshak, A. H. Ph.D. Thesis, Indian Institute of Technology, Rookee, India, 2005.

(24) Reshak, A. H. *J. Chem. Phys.* **2006**, *125*, 014708.

(25) Reshak, A. H. *J. Chem. Phys.* **2006**, *124*, 014707.

(26) Reshak, A. H.; Chen, X.; Auluck, S.; Kityk, I. V. *J. Chem. Phys.* **2008**, *129*, 204111.

JP8098522